ISSN 1674-1056
http://cpb.iphy.ac.cn
http://iopscience.iop.org/cpb
中国物理 B
Chinese Physics
中国物理
Chinese Physics B

Comparison of three kinds of polarized Bessel vortex beams propagating through uniaxial anisotropic media

Jia-Wei Liu(刘佳伟), Hai-Ying Li(李海英), Wei Ding(丁炜), Lu Bai(白璐), Zhen-Sen Wu(吴振森), Zheng-Jun Li(李正军)
Citation: Chin. Phys. B . 2019, 28(9): 094214 . **doi:** 10.1088/1674-1056/28/9/094214
Journal homepage: http://cpb.iphy.ac.cn; http://iopscience.iop.org/cpb

What follows is a list of articles you may be interested in

Soliton guidance and nonlinear coupling for polarized vector spiraling elliptic Hermite-Gaussian beams in nonlocal nonlinear media

Chunzhi Sun(孙春志), Guo Liang(梁果)
Chin. Phys. B . 2019, 28(7): 074206 . **doi:** 10.1088/1674-1056/28/7/074206

Aperture efficiency and mode constituent analysis for OAM vortex beam generated by digital metasurface

Di Zhang(张迪), Xiangyu Cao(曹祥玉), Huanhuan Yang(杨欢欢), Jun Gao(高军), Shiqi Lv(吕世奇)
Chin. Phys. B . 2019, 28(3): 034204 . **doi:** 10.1088/1674-1056/28/3/034204

A new method of calculating the orbital angular momentum spectra of Laguerre-Gaussian beams in channels with atmospheric turbulence

Xiao-zhou Cui(崔小舟), Xiao-li Yin(尹霄丽), Huan Chang(常欢), Zhi-chao Zhang(张志超), Yong-jun Wang(王拥军), Guo-hua Wu(吴国华)
Chin. Phys. B . 2017, 26(11): 114207 . **doi:** 10.1088/1674-1056/26/11/114207

Orbital angular momentum density and spiral spectra of Lorentz-Gauss vortex beams passing through a single slit

Zhi-Yue Ji(季志跃), Guo-Quan Zhou(周国泉)
Chin. Phys. B . 2017, 26(9): 094202 . **doi:** 10.1088/1674-1056/26/9/094202

Microscale vortex laser with controlled topological charge

Xing-Yuan Wang(王兴远), Hua-Zhou Chen(陈华洲), Ying Li(黎颖), Bo Li(李波), Ren-Min Ma(马仁敏)
Chin. Phys. B . 2016, 25(12): 124211 . **doi:** 10.1088/1674-1056/25/12/124211

Comparison of three kinds of polarized Bessel vortex beams propagating through uniaxial anisotropic media*

Jia-Wei Liu(刘佳伟), Hai-Ying Li(李海英)†, Wei Ding(丁炜), Lu Bai(白璐), Zhen-Sen Wu(吴振森), and Zheng-Jun Li(李正军)

School of Physics and Optoelectronic Engineering, Xidian University, Xi'an 710126, *China*

(Received 8 May 2019; revised manuscript received 10 July 2019; published online 23 August 2019)

A comparison of differently polarized Bessel vortex beams propagating through a uniaxial anisotropic slab is discussed in terms of the vector wave function expansions. The magnitude profiles of electric field components, the transformation of polarization modes, and the distributions of orbital angular momentum (OAM) states of the reflected and transmitted beams for different incident angles are numerically simulated. The results indicate that the magnitude profiles of electric field components for different polarization modes are distinct from each other and have a great dependence on the incident angle, thus the transformation of polarization modes which reflects the change of energy can be affected largely. As compared to the x and circular polarization incidences, the reflected and transmitted beams for the radial polarization incidence suffer the fewest transformation of polarization modes, showing a better energy invariance. The distributions of OAM states of the reflected and transmitted beams for different polarization modes are diverse as well, and the derived OAM states of the transmitted beam for radial polarization present a focusing effect, concentrating on the state between two predominant OAM states.

Keywords: orbital angular momentum, Bessel vortex beams, reflection and transmission, polarization

PACS: 42.25.Bs, 78.20.Ci, 13.88.+e **DOI:** 10.1088/1674-1056/ab37f5

1. Introduction

The vortex beams carrying orbital angular momentum (OAM)[1] have been widely studied over a few past decades, including generation,[2,3] characteristics,[4–6] and applications in optical communication,[7] imaging,[8] microparticle manipulation,[9] *etc*. In particular, the different OAM states are mutually orthogonal while propagating coaxially and thus promote potential applications in improving the capacity of communication systems. Gibson *et al.* implemented the initial demonstration of using OAM for free-space communication, experimentally proving the possibility of transmitting information by vortex beams.[10] The team led by Wang has been working on the multiplex/demultiplex of OAM in the optical band and has obtained several valuable research results.[11,12] Appreciable literatures on the transmission efficiency,[13–15] the security performance,[16] and the mitigation of crosstalk[17] of vortex beams have been reported. Some other researches which are worth mentioning also boost the development of vortex beams in quantum communication,[18] RF communication,[19] and material processing.[20] Whereas, the propagation of vortex beams in media inevitably results in the distortion of electric field amplitude and further causes the crosstalk of OAM states.[21] Such distortion is even serious in anisotropic media because of the double refraction behavior. Yu[22] and Wang[23] studied the propagation of Airy Gaussian vortex beams and chirped Airy vortex beams in uniaxial crystals, respectively. The results prove that the ratio of extraordinary and ordinary refractive indices affects the asymmetry of the intensity a lot. As a kind of typical anisotropic media, uniaxial anisotropic media are widely applied in optical signal processing,[24] optical element design,[25] and manufacturing of microwave devices.[26] Exploring the variations of field profile, polarization mode, and OAM state of the reflected and transmitted beams during the propagation of vortex beams in uniaxial media can potentially improve the quality and efficiency of practical applications.[27]

Compared to other vortex beams, Bessel vortex beams[28] whose electric field intensity is independent of propagation distance are treated to be more advantageous for long-distance communication,[29] optical imaging,[30] and other applications[31,32] since its field profile can self-reconstruct after passing through obstacles. Besides, such diffraction-free beams suffer less power loss than Gaussian beams,[33] which means a higher signal-noise ratio in practical optical communication. With the need of large data transmission for optical communication, according to the Fresnel–Arago interference law,[34] the general way is to use the same information-carrying beams with two orthogonal linear polarization modes at the input of an optical communication system to provide twofold data channels.[35] However, it will lower the transmis-

*Project supported by the National Natural Science Foundation of China (Grant Nos. 61801349, 61875156, and 61571355) and the 111 Project, China (Grant No. B17035).

†Corresponding author. E-mail: lihy@xidian.edu.cn

© 2019 Chinese Physical Society and IOP Publishing Ltd

sion efficiency of communication systems because there must be corresponding polarizers at the receiving end to decode the information carried by beams with different linear polarization modes. A high extinction ratio polarization beam splitter skillfully utilizing the displacements of TE- and TM-polarized beams in a low-symmetric photonic crystal was designed to simplify the optical communication system in the precondition of high transmission efficiency.[36] Furthermore, Quabis *et al.* found that the radially polarized beams have the favorable focusing characteristic which could be used to build improved near field sensors.[37] Generally speaking, the polarized Bessel vortex beams (PBVBs) which simultaneously possess the polarization characteristics and OAM properties are potential to increase information capacity and transmission efficiency by combining with the polarization–division multiplexing (PDM) and mode–division multiplexing (MDM) systems. However, in this case, the distortion of electric fields and the crosstalk of OAM states stemming from the transformation of polarization modes need to be taken into account. As far back as 2001, Nesterov and Niziev had investigated the propagation characteristics of beams with axially symmetric polarization, finding that such polarized beams are free from polarization aberrations.[38] King also found the derivation of topological charge of a circularly polarized Bessel vortex beam in biaxial crystals and demonstrated the transformation of a Bessel beam from zeroth to first order and then from first to second order.[39] Furthermore, the oscillating polarization along the optical axis of Bessel beams in free space was discussed by Fu and his co-worker.[40] It seems that the influence of polarization mode on the propagation of a Bessel vortex beam is still worth considering for further understanding, especially in the communication systems involving both polarization–division multiplexing and OAM–division multiplexing.

In this paper, the comparison of three kinds of polarized Bessel vortex beams incident on a uniaxial anisotropic slab is investigated by use of the cylindrical vector wave function expansions and the eigen plane wave spectrum representation. The paper is arranged as follows: Section 2 gives the expressions of the incident, reflected, and transmitted fields, as well as the field in the internal slab in terms of the cylindrical vector wave functions (CVWFs). On this basis, the reflected and transmitted field components are simulated numerically and discussed in Section 3, including the transformation of polarization modes and the OAM state distribution of the reflected and transmitted beams for different incident angles and for different polarization modes. Section 4 presents the conclusions.

2. Theoretical background

The sketch of an arbitrary polarized Bessel vortex beam which is obliquely incident on a uniaxial anisotropic slab is shown in Fig. 1. Figure 1(a) is the graphic model and describes the geometrical relationship between the global system and the local coordinate systems. The origins of the incident and reflected coordinate systems ($Ox_iy_iz_i$ and $Ox_ry_rz_r$) coincide with those of the global coordinate system. The outgoing point of ordinary wave in slab is chosen as the origin of the transmitted coordinate system $O'x_ty_tz_t$ for the convenience of estimating the displacement by Snell's law. The incident angle and the thickness of slab are β and d, respectively. In this paper, the time-harmonic factor is $\exp(-\mathrm{i}\omega t)$.

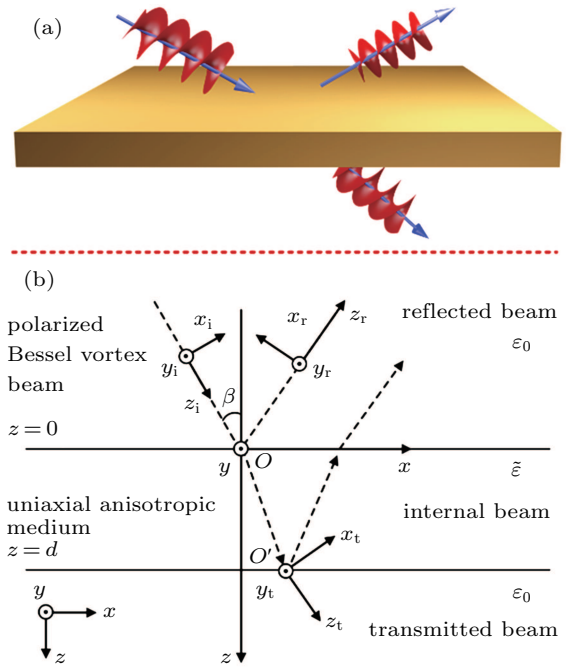


Fig. 1. Oblique incidence of an arbitrarily polarized Bessel vortex beam on a uniaxial anisotropic slab.

According to the angular spectrum decomposition (ASD) method, the electric and magnetic field vectors of a polarized Bessel vortex beam under the incident coordinate system $Ox_iy_iz_i$ are expressed as[41]

$$\begin{aligned}\boldsymbol{E}(\boldsymbol{r}) &= \int_{\beta'=0}^{2\pi} E_{\mathrm{pw0}}\, \boldsymbol{Q}|_{\alpha'=\alpha_0}\, \mathrm{e}^{\mathrm{i}l\beta'}\, \mathrm{e}^{\mathrm{i}\boldsymbol{k}\cdot(\boldsymbol{r}-\boldsymbol{r}_0)}\mathrm{d}\beta',\\ \boldsymbol{H}(\boldsymbol{r}) &= \int_{\beta'=0}^{2\pi} E_{\mathrm{pw0}}\frac{k}{\mu_0\omega}\boldsymbol{k}\times\boldsymbol{Q}|_{\alpha'=\alpha_0}\, \mathrm{e}^{\mathrm{i}l\beta'}\, \mathrm{e}^{\mathrm{i}\boldsymbol{k}\cdot(\boldsymbol{r}-\boldsymbol{r}_0)}\mathrm{d}\beta', \quad (1)\end{aligned}$$

where $\boldsymbol{r}_0 = (x_0, y_0, z_0)$ corresponds to the position of beam center in the global coordinate system, which is set to $\boldsymbol{r}_0 = (0,0,0)$. $\boldsymbol{k}$ is the wave vector. The notations l and α_0 are the topological charge and the half cone angle of the incident beam, respectively. E_{pw0} is the amplitude of the electric field of the plane waves propagating over a cone. α' and β' denote, respectively, the polar and azimuthal angles of the wave vector under the incident coordinate system. ω is the circular frequency. The complex polarization function $\boldsymbol{Q}$ for arbitrary polarization is written as[42]

$$\boldsymbol{Q} = \begin{bmatrix} p_{x_\mathrm{i}}(\cos\alpha'\cos^2\beta' + \sin^2\beta') - p_{y_\mathrm{i}}(1-\cos\alpha')\sin\beta'\cos\beta' \\ p_{x_\mathrm{i}}(\cos\alpha'-1)\sin\beta'\cos\beta' + p_{y_\mathrm{i}}(\cos\alpha'\sin^2\beta' + \cos^2\beta') \\ -p_{x_\mathrm{i}}\sin\alpha'\cos\beta' - p_{y_\mathrm{i}}\sin\alpha'\sin\beta' \end{bmatrix} \begin{Bmatrix} e_{x_\mathrm{i}} \\ e_{y_\mathrm{i}} \\ e_{z_\mathrm{i}} \end{Bmatrix}, \tag{2}$$

with $(p_{x_\mathrm{i}}, p_{y_\mathrm{i}})$ being the complex polarization parameters. $\boldsymbol{e}_{(x_\mathrm{i},y_\mathrm{i},z_\mathrm{i})}$ are unit vectors of the Cartesian incident system. Specifically, $(p_{x_\mathrm{i}}, p_{y_\mathrm{i}}) = (1,0)$, $(1,\mathrm{i})$, $(\cos\beta', \sin\beta')$ stands for the x polarization, the circular polarization (left-hand in this paper), and the radial polarization, respectively.

By expanding the factor $\boldsymbol{Q}|_{\alpha'=\alpha_0}\,\mathrm{e}^{\mathrm{i}\boldsymbol{k}\cdot\boldsymbol{r}}$ in terms of the spherical vector wave functions (SVWFs), the electric and magnetic field vectors of a PBVB can be expressed as[43]

$$\begin{aligned} \boldsymbol{E} &= E_0 \sum_{n=1}^{\infty}\sum_{m=-n}^{n} \left[a_{mn}\mathrm{M}_{mn}^{(1)}(kr_\mathrm{i},\theta_\mathrm{i},\phi_\mathrm{i}) \right. \\ &\quad \left. + b_{mn}\mathrm{N}_{mn}^{(1)}(kr_\mathrm{i},\theta_\mathrm{i},\phi_\mathrm{i})\right], \\ \boldsymbol{H} &= E_0 \frac{k}{\mathrm{i}\omega\mu_0} \sum_{n=1}^{\infty}\sum_{m=-n}^{n} \left[a_{mn}\mathrm{N}_{mn}^{(1)}(kr_\mathrm{i},\theta_\mathrm{i},\phi_\mathrm{i}) \right. \\ &\quad \left. + b_{mn}\mathrm{M}_{mn}^{(1)}(kr_\mathrm{i},\theta_\mathrm{i},\phi_\mathrm{i})\right], \end{aligned} \tag{3}$$

where $\mathrm{M}_{mn}^{(1)}(kr_\mathrm{i},\theta_\mathrm{i},\phi_\mathrm{i})$ and $\mathrm{N}_{mn}^{(1)}(kr_\mathrm{i},\theta_\mathrm{i},\phi_\mathrm{i})$ are the SVWFs belonging to the incident coordinate system, and the superscript (1) represents the spherical Bessel function of the first kind. The expansion coefficients a_{mn} and b_{mn} are as follows:

$$\begin{aligned} a_{mn} &= -4\mathrm{i}^{n+1}D_{mn}\,\mathrm{e}^{-\mathrm{i}k_{z_\mathrm{i}}z_0}\left[\pi_{mn}(\cos\alpha_0)I_+ + \tau_{mn}(\cos\alpha_0)I_-\right], \\ b_{mn} &= -4\mathrm{i}^{n+1}D_{mn}\,\mathrm{e}^{-\mathrm{i}k_{z_\mathrm{i}}z_0}\left[\tau_{mn}(\cos\alpha_0)I_+ + \pi_{mn}(\cos\alpha_0)I_-\right], \end{aligned} \tag{4}$$

where I_+ and I_- are the coefficients shown in Ref. [43], $D_{mn} = (2n+1)(n-m)!/4n(n+1)(n+m)!$. π_{mn} and τ_{mn} are the angle functions.

Considering the incident angle β, by utilizing the addition theorem of the SVWFs, the electric field vector of the incident beam can be expressed under the global coordinate system $Oxyz$ as[44]

$$\begin{aligned} \boldsymbol{E}^\mathrm{i} &= E_0 \sum_{n=1}^{\infty}\sum_{m=-n}^{n} \left[a'_{mn}\mathrm{M}_{mn}^{(1)}(kr,\theta,\phi) \right. \\ &\quad \left. + b'_{mn}\mathrm{N}_{mn}^{(1)}(kr,\theta,\phi)\right], \end{aligned} \tag{5}$$

where $\mathrm{M}_{mn}^{(1)}(kr,\theta,\phi)$ and $\mathrm{N}_{mn}^{(1)}(kr,\theta,\phi)$ are the SVWFs belonging to $Oxyz$. Here, the superscript i refers to the incident beam. The expansion coefficients a'_{mn} and b'_{mn} are

$$(a'_{mn}, b'_{mn}) = \sum_{s=-n}^{n} \rho(s,m,n)(a_{sn}, b_{sn}) \tag{6}$$

and the specific expression of $\rho(m,s,n)$ can be found in Ref. [45].

According to the transformation relationship between the SVWFs and the CVWFs,[44] equation (5) can be rewritten by means of the CVWFs as

$$\begin{aligned} \boldsymbol{E}^\mathrm{i} &= E_0 \sum_{m=-\infty}^{\infty}\int_0^{\pi} \left[A_m(\zeta)\,\mathrm{m}_{m\lambda}^{(1)}(h) \right. \\ &\quad \left. + B_m(\zeta)\,\mathrm{n}_{m\lambda}^{(1)}(h)\right]\mathrm{e}^{\mathrm{i}hz}\mathrm{d}\zeta, \end{aligned} \tag{7}$$

where $\mathrm{m}_{m\lambda}^{(1)}$ and $\mathrm{n}_{m\lambda}^{(1)}$ are the CVWFs belonging to the global coordinate system. $\lambda = k\sin\zeta$, $h = k\cos\zeta$, $\boldsymbol{k} = \lambda\hat{\rho} + h\hat{z}$. ζ is the angle between the wave vector $\boldsymbol{k}$ and the z axis. The corresponding expansion coefficients $A_m(\zeta)$ and $B_m(\zeta)$ are as follows:

$$\begin{aligned} A_m(\zeta) &= \sum_{n=|m|}^{\infty}\left[a'_{mn}c_{mn}(\zeta) + b'_{mn}d_{mn}(\zeta)\right], \\ B_m(\zeta) &= \sum_{n=|m|}^{\infty}\left[a'_{mn}d_{mn}(\zeta) + b'_{mn}c_{mn}(\zeta)\right], \end{aligned} \tag{8}$$

where

$$c_{mn} = -\frac{\mathrm{i}^{m-n+1}}{2k}\tau_{mn}(\cos\zeta), \quad d_{mn} = \frac{\mathrm{i}^{m-n-1}}{2k}\pi_{mn}(\cos\zeta). \tag{9}$$

The corresponding expansion for the magnetic field vector can be obtained by Maxwell equations.

Let us consider the actual incidence of a PBVB which can be interpreted as the superposition of plane wavelets. Under this proposition, only the plane wavelets which illuminate on the upper surface of the slab are considerable, which means that the integration interval of ζ in Eq. (7) is from 0 to $\pi/2$.

Similarly, the electric field vectors of the reflected and transmitted beams are as follows:

$$\begin{aligned} \boldsymbol{E}^\mathrm{r} &= E_0 \sum_{m=-\infty}^{\infty}\int_0^{\pi/2} \left[C_m(\zeta)\,\mathrm{m}_{m\lambda}^{(1)}(-h) \right. \\ &\quad \left. + D_m(\zeta)\,\mathrm{n}_{m\lambda}^{(1)}(-h)\right]\mathrm{e}^{-\mathrm{i}hz}\mathrm{d}\zeta, \end{aligned} \tag{10}$$

$$\begin{aligned} \boldsymbol{E}^\mathrm{t} &= E_0 \sum_{m=-\infty}^{\infty}\int_0^{\pi/2} \left[G_m(\zeta)\,\mathrm{m}_{m\lambda}^{(1)}(h) \right. \\ &\quad \left. + I_m(\zeta)\,\mathrm{n}_{m\lambda}^{(1)}(h)\right]\mathrm{e}^{\mathrm{i}hz}\mathrm{d}\zeta, \end{aligned} \tag{11}$$

where the superscripts r and t are the symbols of the reflected and transmitted beams, respectively. $\{C_m(\zeta), D_m(\zeta)\}$ and $\{G_m(\zeta), I_m(\zeta)\}$ are the corresponding expansion coefficients.

The electric field of the internal beam in a uniaxial anisotropic slab whose optic axis is perpendicular to the upper surface ($\tilde{\varepsilon} = \varepsilon_\mathrm{t}\boldsymbol{e}_x\boldsymbol{e}_x + \varepsilon_\mathrm{t}\boldsymbol{e}_y\boldsymbol{e}_y + \varepsilon_z\boldsymbol{e}_z\boldsymbol{e}_z$ is the permittivity) is given by the Fourier transform and the eigen plane wave spectrum representation[46]

$$\begin{aligned} \boldsymbol{E}_1^\mathrm{w} &= E_0 \sum_{q=1}^{2}\sum_{m=-\infty}^{\infty}\int_0^{\pi/2} E_{mq}(\zeta)\left[\alpha_q(\zeta)\,\mathrm{m}_{m\lambda}^{(1)}(h_q) \right. \\ &\quad \left. + \beta_q(\zeta)\,\mathrm{n}_{m\lambda}^{(1)}(h_q) + \gamma_q(\zeta)\,\mathrm{l}_{m\lambda}^{(1)}(h_q)\right]\mathrm{e}^{\mathrm{i}h_q z}\mathrm{d}\zeta, \end{aligned} \tag{12}$$

$$\begin{aligned} \boldsymbol{E}_2^\mathrm{w} &= E_0 \sum_{q=1}^{2}\sum_{m=-\infty}^{\infty}\int_0^{\pi/2} F_{mq}(\zeta)\left[\alpha_q(\zeta)\,\mathrm{m}_{m\lambda}^{(1)}(-h_q) \right. \\ &\quad \left. + \beta_q(\zeta)\,\mathrm{n}_{m\lambda}^{(1)}(-h_q) - \gamma_q(\zeta)\,\mathrm{l}_{m\lambda}^{(1)}(-h_q)\right]\mathrm{e}^{-\mathrm{i}h_q z}\mathrm{d}\zeta, \end{aligned} \tag{13}$$

where the coefficients α_q, β_q, and γ_q can be found in Ref. [46]. The superscript w denotes the internal beam, and the subscripts 1 and 2 refer to the down- and up-going waves, respectively. The integer indices $q = 1, 2$ give the explanation to the double refraction behavior of a uniaxial anisotropic slab. E_{mq} and F_{mq} are the expansion coefficients.

Through the electromagnetic fields boundary conditions that the tangential components of the electromagnetic fields are continuous, a set of simultaneous equations can be obtained, from which the expansion coefficients and then the corresponding field components can be solved numerically.

To analyze the effects of such media on the transformation of polarization modes during the propagation of a PBVB, the following expression[47] which is similar to the definition of the polarization extinction ratio (PER) is used to investigate the polarization characteristics of the reflected and transmitted beams:

$$\mathrm{Pol} = 10\lg \frac{\iint S_{z\xi,x\xi}\,\mathrm{d}x_\xi \mathrm{d}y_\xi}{\iint S_{z\xi,y\xi}\,\mathrm{d}x_\xi \mathrm{d}y_\xi}, \quad (\xi = \mathrm{r,t}), \tag{14}$$

where $\xi = \mathrm{r,t}$ stand for the reflected and transmitted beams, respectively. $S_{z\xi,x\xi}$ denotes the longitudinal component of the time-average Poynting vector power density resulted from the electric field component $E_{x\xi}$, with $S_{z\xi,y\xi}$ corresponding the electric field component $E_{y\xi}$.

Similar to the angular spectrum decomposition, vortex beams can be interpreted as the superposition of infinite spiral harmonics $\exp(\mathrm{i}n\phi)$ according to the expansion of spiral spectrum.[48] n is the integer index and ϕ stands for the phase factor. In this way, the field components of the reflected and the transmitted beams can be expressed as follows:

$$U\left(r_\xi, \phi_\xi, z_\xi\right) = \frac{1}{\sqrt{2\pi}} \sum_{n=-\infty}^{\infty} s_n\left(r_\xi, z_\xi\right) \exp(\mathrm{i}n\phi_\xi), \tag{15}$$

where U refers to the electric field components $\{E_{x\xi}, E_{y\xi}, E_{z\xi}\}$ or the magnetic field components $\{H_{x\xi}, H_{y\xi}, H_{z\xi}\}$, and the coefficient $s_n(r_\xi, z_\xi)$ means the amplitude of the corresponding spiral harmonic component and can be expressed as

$$s_n\left(r_\xi, z_\xi\right) = \frac{1}{\sqrt{2\pi}} \int_0^{2\pi} U\left(r_\xi, \phi_\xi, z_\xi\right) \mathrm{e}^{-\mathrm{i}n\phi_\xi}\,\mathrm{d}\phi_\xi. \tag{16}$$

As we all know that the time-averaged energy density of a beam is $\langle w\rangle = [\varepsilon_0 \boldsymbol{E}\cdot\boldsymbol{E}^* + \boldsymbol{B}\cdot\boldsymbol{B}^*/\mu_0]/16\pi$, where ε_0 and μ_0 are the permittivity and the permeability of vacuum, respectively. Substituting Eq. (16) into the time-averaged energy density expression, we finally arrive at the weight function of OAM states

$$P_{n\xi} = \frac{\int \langle w_n\rangle\, r_\xi \mathrm{d}r_\xi}{\sum_{-\infty}^{\infty} \int \langle w_n\rangle\, r_\xi \mathrm{d}r_\xi}. \tag{17}$$

3. Numerical simulations and discussion

To intuitively analyze the influence of the incident angle and polarization on the deformations of the electric field amplitude and OAM state, as well as the transformation of polarization mode, numerical simulations are given below by using the theoretical formulae derived in Section 2. The wavelength is $\lambda_0 = 0.6328$ μm. The half-cone angle and the topological charge of the incident PBVB are set as $\alpha_0 = 10^\circ$ and $l = 2$, respectively. The parameters of the uniaxial anisotropic slab are as follows: $d = 10\lambda_0$, $\varepsilon_\mathrm{t} = 2.7502$, and $\varepsilon_z = 2.2094$ (Calcite).

3.1. Comparison of magnitude profiles of electric field components of the incident, reflected, and transmitted beams

Figure 2 shows the magnitude profiles of the incident electric field components. The row-panels represent the polarization modes, *i.e.*, x polarization (x polar.), circular polarization (circ polar.), and radial polarization (rad. polar.), from up to down, respectively) of the incident beam, and the column-panels stand for the electric field components (E_{x_i}, E_{y_i} and E_{z_i} from left to right, respectively). Such results bring into correspondence with the numerical simulations in Ref. [49], proving the reasonability of the method used in this paper.

As we can see from Fig. 2 that the electric field component E_{x_i} is prominent in the case of x polarization with a circular symmetric structure. For circular polarization incidence, all of the electric field components keep circular symmetry and the transverse electric field components E_{x_i} and E_{y_i} have the same magnitude profiles. Although the longitudinal electric component E_{z_i} maintaining circular symmetry for radial polarization incidence, the transverse electric field components both have an axial symmetric crescent contour.

The magnitude profiles of electric field components of the reflected beam for different polarization modes are displayed in Figs. 3–5. Each figure includes 9 panels, where the row-panels represent the cases of different incident angles (10°, 20°, and 30° from up to down, respectively) and the column-panels represent the electric field components (E_{x_r}, E_{y_r} and E_{z_r} from left to right, respectively).

It can be seen from Figs. 3–5 that as the incident angle increases, the contours of the reflected field components for all three kinds of polarization modes are seriously distorted, associating with a gradually increasing displacement along the negative x_r axis. It is because that the reflected beam contains the beams reflected by both upper and lower surfaces of the slab, these beams superimpose together resulting in the more deformed contours. Such a process occurs in the transmitted beams too, but the low reflectance mitigates the distortion caused by the superimposition. In addition, the magnitudes of electric field components E_{x_r} decrease, which are just opposite to the electric field component E_{y_r}. The magnitude profile of the electric field component E_{x_r} for the x polarization incidence is similar to the components E_{x_r} and E_{y_r} for the circular polarization incidence, as well as the changing trend with the increasing incident angle just as figures 3 and 4 show.

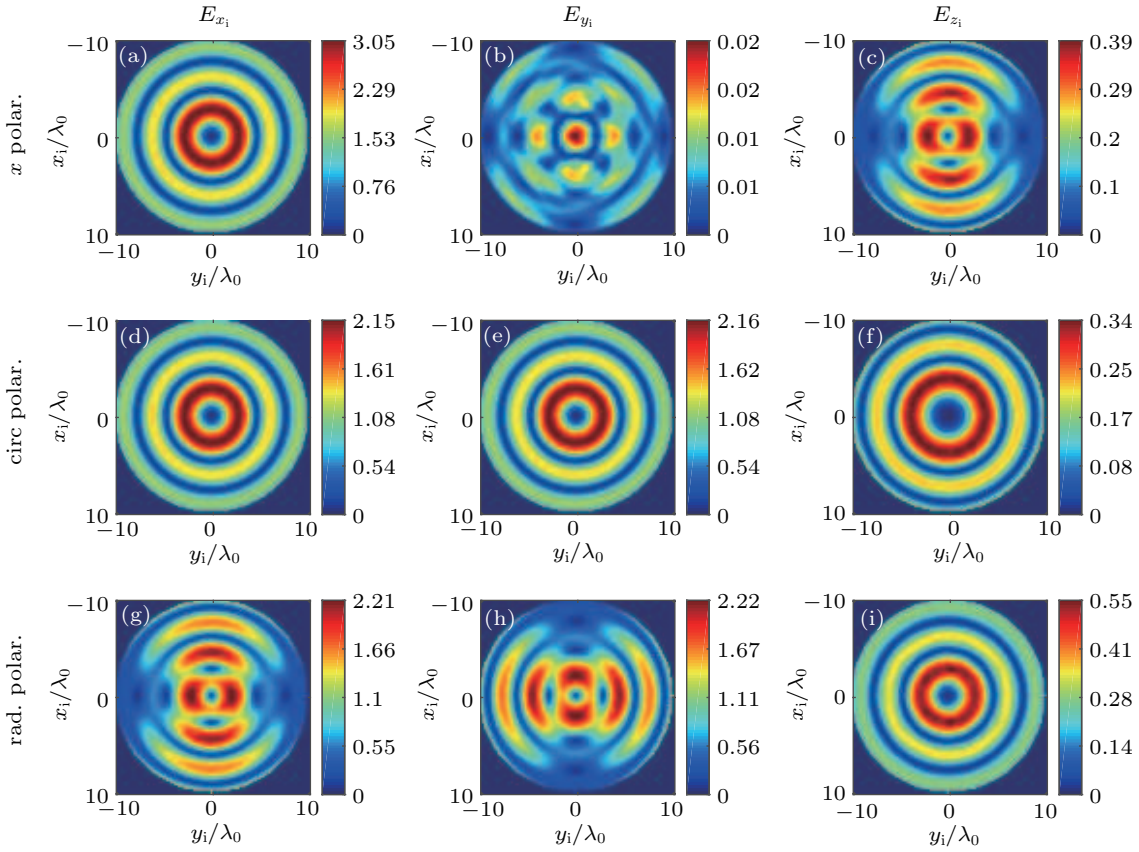


Fig. 2. Magnitude profiles of the electric field components of incident beam for different polarization modes.

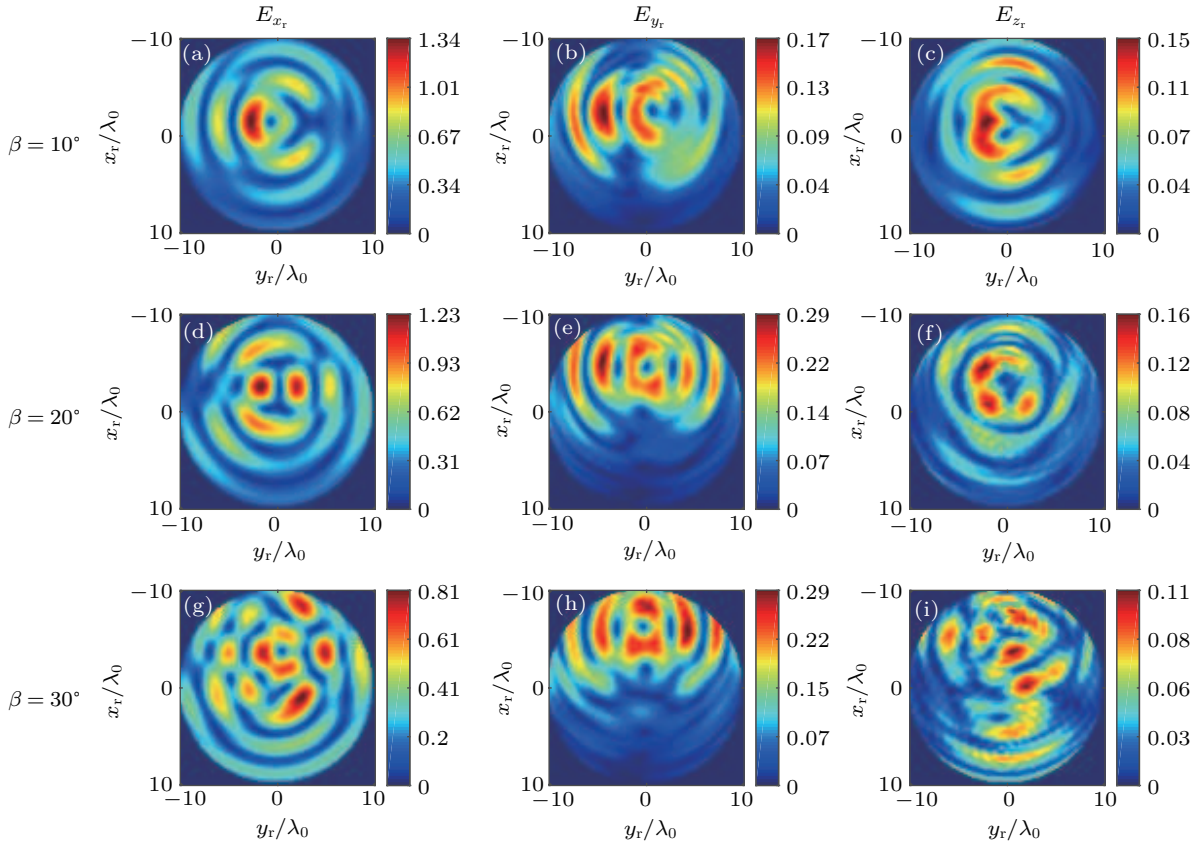


Fig. 3. Magnitude profiles of the reflected electric field components for the x polarized incidences.

Compared to the circular polarization incidence, the difference between the maximum values of the transverse electric field components E_{x_r} and E_{y_r} for the radial polarization incidence is smaller, which means that there are fewer changes for the

polarization mode. Furthermore, the reflected beam for such polarization incidence has the biggest longitudinal electric field component as shown in Fig. 5.

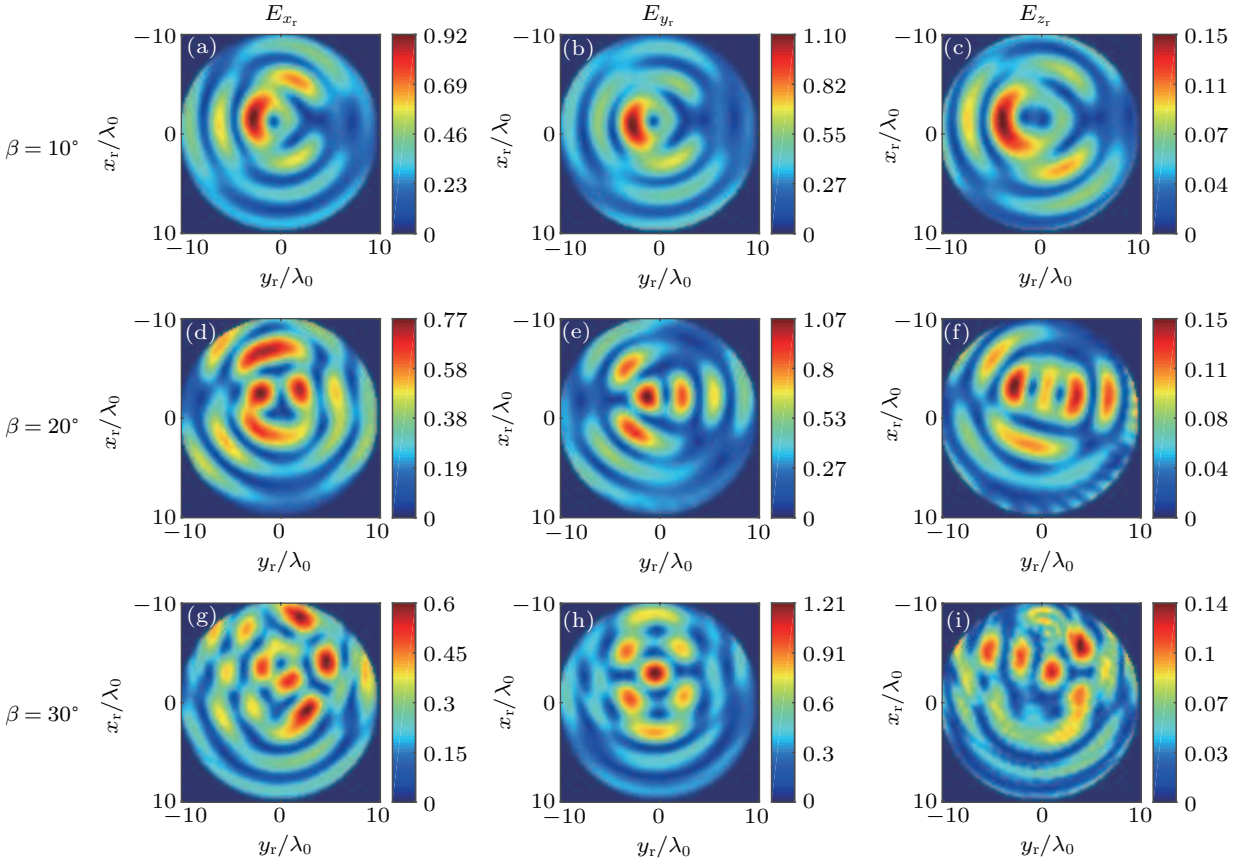


Fig. 4. Magnitude profiles of the reflected electric field components for the circularly polarized incidence.

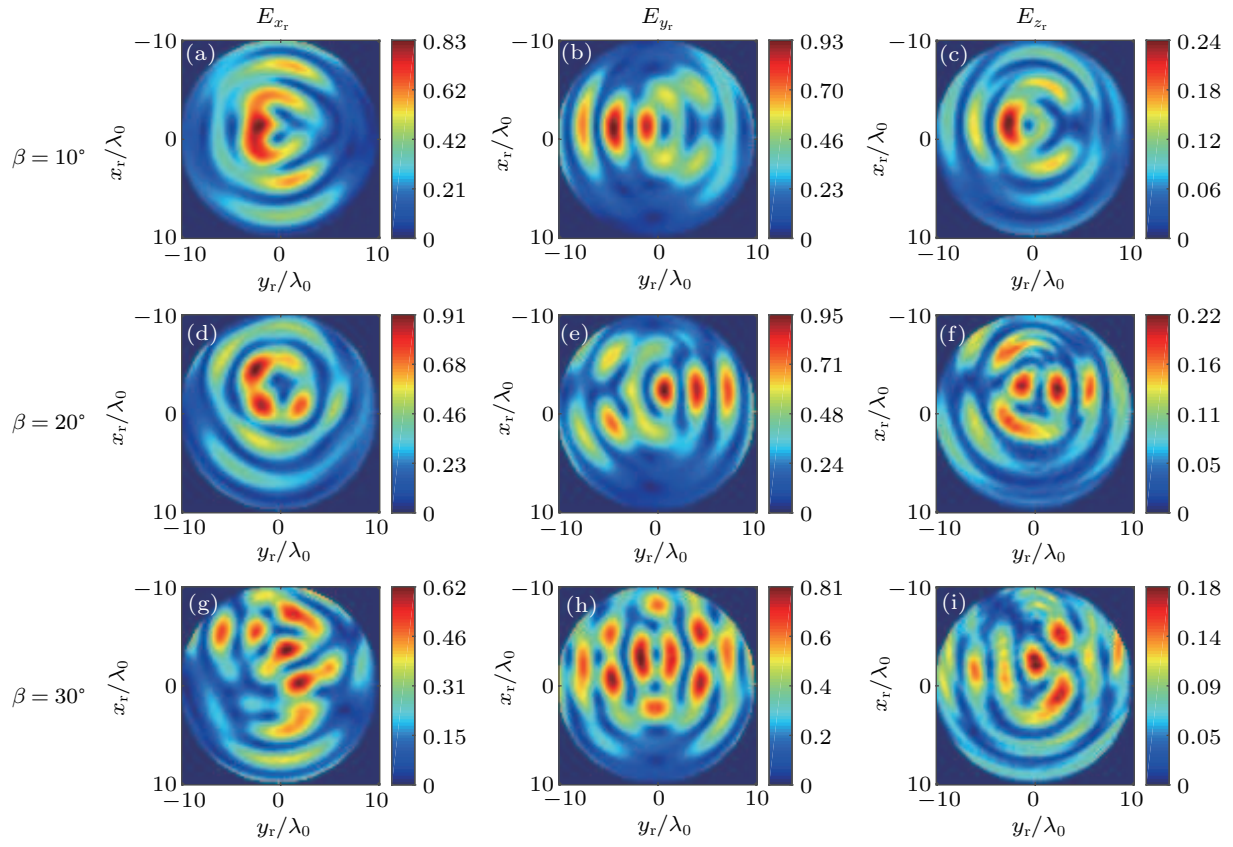


Fig. 5. Magnitude profiles of the reflected electric field components for the radially polarized incidence.

Similarly, the magnitude profiles of electric field components of the transmitted beam are presented in Figs. 6–8, where the row-panels also represent the cases of different incident angles and the column-panels represent the transmitted electric field components (E_{x_t}, E_{y_t}, and E_{z_t} from left to right, respectively).

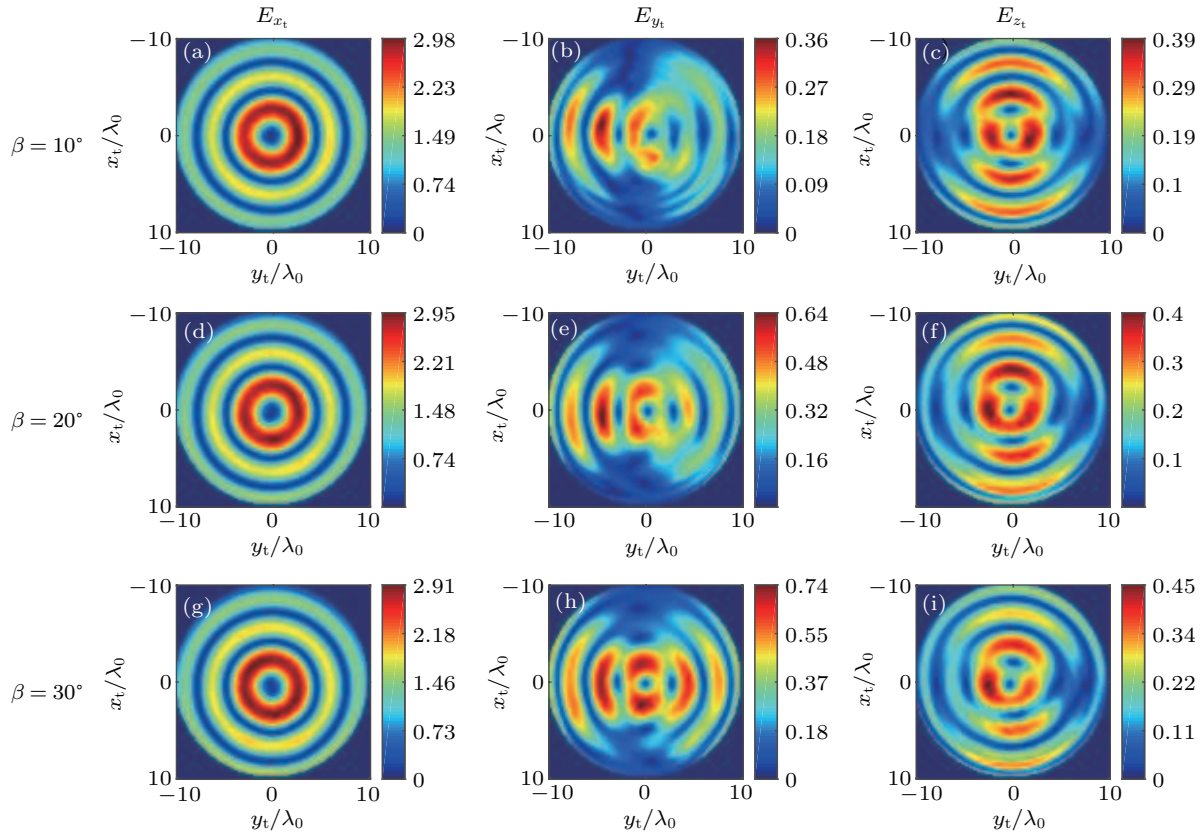


Fig. 6. Magnitude profiles of the transmitted electric field components for the x polarized incidence.

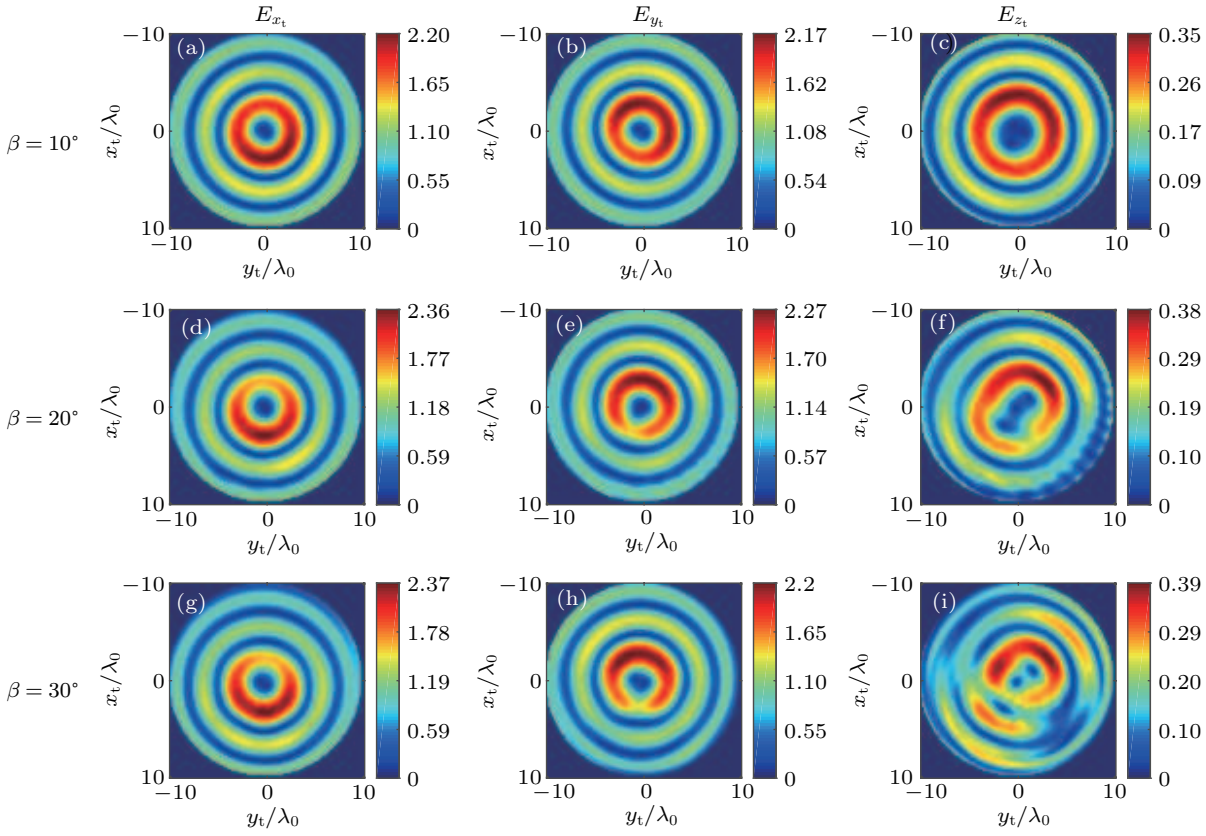


Fig. 7. Magnitude profiles of the transmitted electric field components for the circularly polarized incidence.

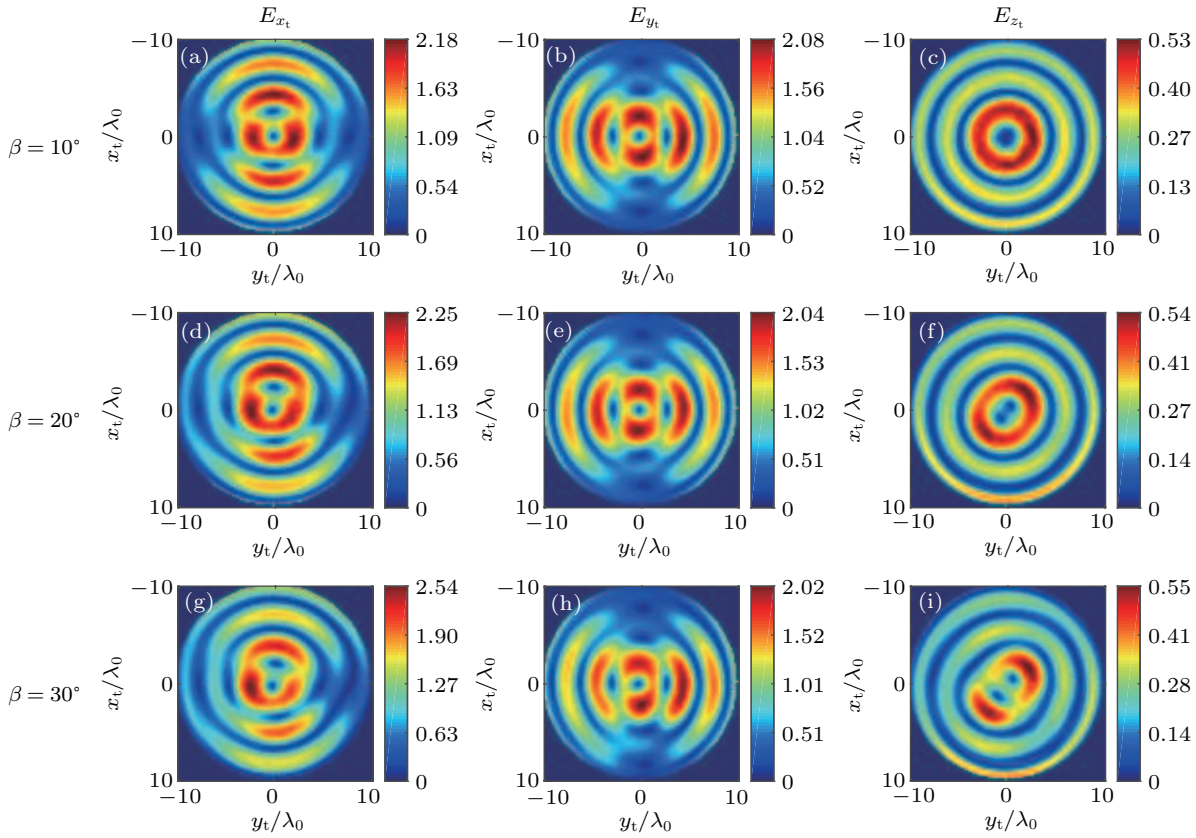


Fig. 8. Magnitude profiles of the transmitted electric field components for the radially polarized incidence.

Just as the behaviors of reflected field components, the magnitude profiles of the transmitted field components also have distortions. Comparing with the incident beams, the central circular rings in the contours shown in Figs. 6–8 have changed significantly, especially for the circular polarization incidence. Meanwhile, as the incident angle increases, the distortion of the central ring is more remarkable. Figure 7 shows the appearance of a rotation in 180° in the contour variations of the central circular rings in both E_{xt} and E_{yt}.

To have a clear understanding about the variations of the polarization of the reflected and transmitted beams, the value of Pol by Eq. (14) is used to analyze the transformation of polarization modes.

3.2. Transformation of polarization modes of the reflected and transmitted beams

In order to provide a reference for comparison, the polarization patterns of the incident beams are presented in Fig. 9.

Figure 9 indicates that the electric field vectors of the incident beam with the x polarization are along the x_i axis, and for the circular polarization, the electric field vectors form the shape of a hexagonal star whose points are located at infinity. The polarization pattern of the radially polarized incident beam is more intricate. The electric field vectors outside the second bright ring are along the radial direction. Inside the second bright ring, the electric field vectors start from two source points and disappear in the other two end points as figure 9(c) shows.

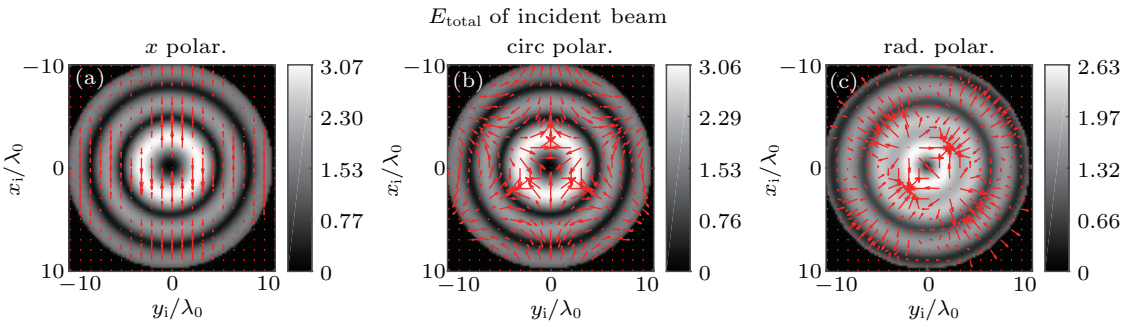


Fig. 9. Polarization patterns of the incident beam: (a) x polarization; (b) circular polarization; (c) radial polarization.

Figures 10 and 11 show the polarization patterns of the reflected and transmitted beams for different incident angles. The row-panels represent the cases of polarization modes (x, circular, and radial polarizations from up to down, respectively), and the

column-panels stand for the cases of different incident angles (10°, 20°, and 30° from left to right, respectively).

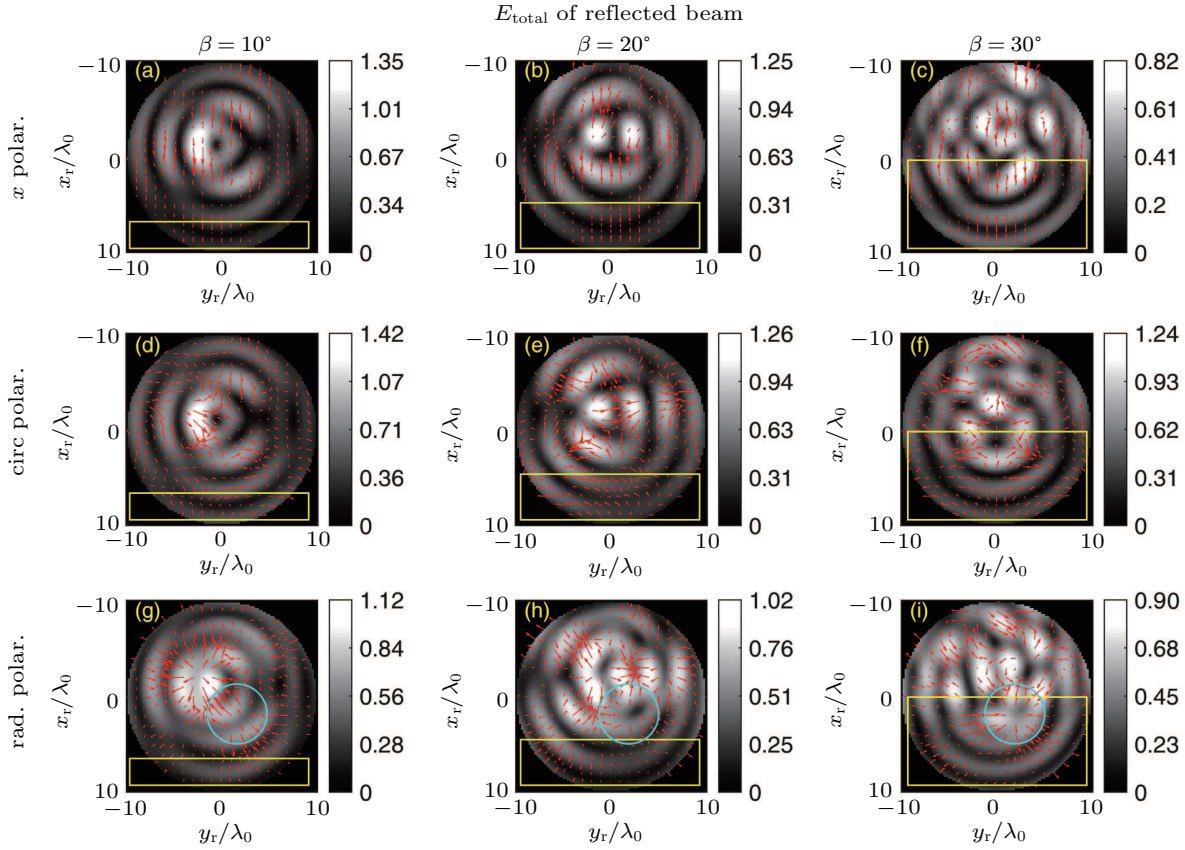


Fig. 10. Polarization patterns of the reflected beam with different incident angles.

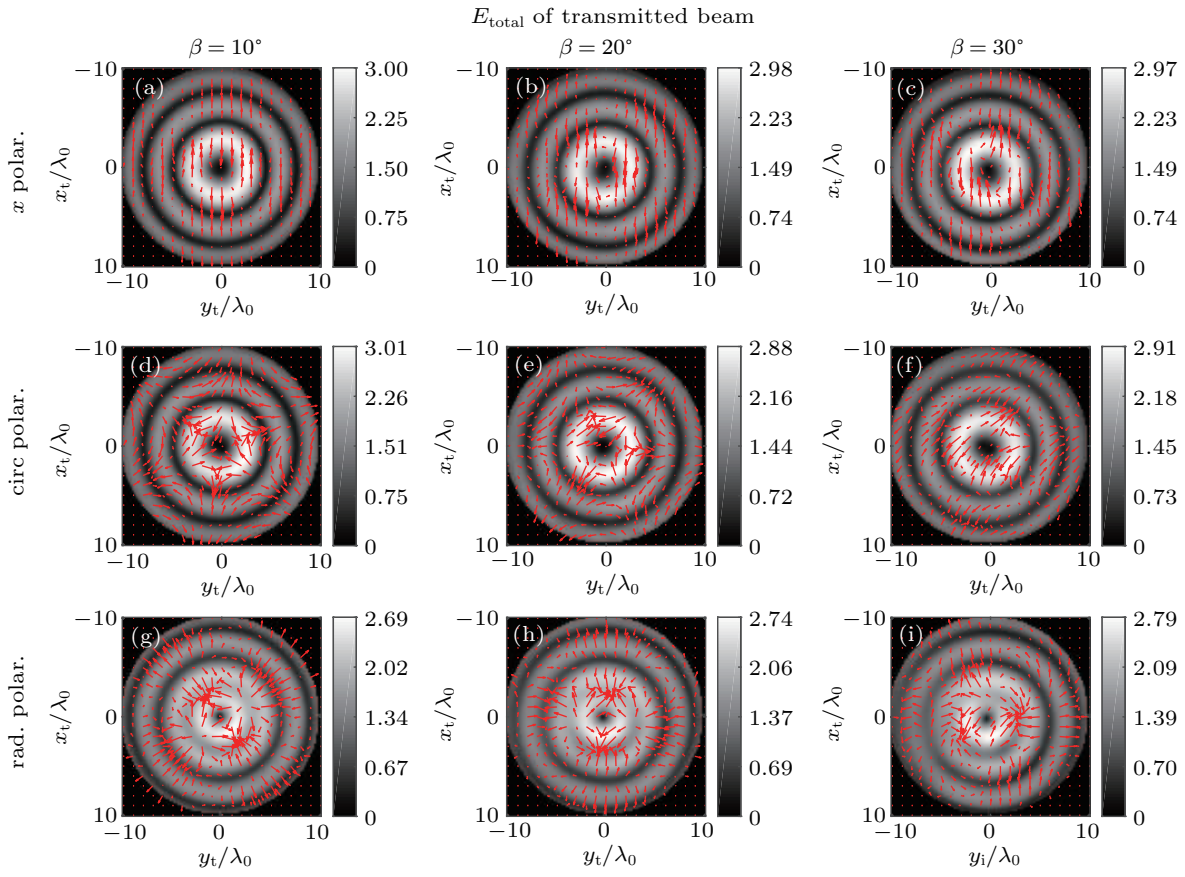


Fig. 11. Polarization patterns of the transmitted beam with different incident angles.

It can be seen from Figs. 10 and 11 that the original polarization modes are largely destroyed after reflection. However, the electric field vectors inside the yellow rectangle are similar to the polarization pattern of the incident beam when the incident angle is 30°, showing better resilience as the incident angle increases. It reveals that the direction of electric field vectors inside the blue circle is comparable to that of the incident beam in Fig. 9(c) when the incident angle equals 30° as shown in Fig. 10(i). At the same incident angle, the electric field vectors of the reflected beam are more rambling compared with those of the transmitted beam, and the polarization patterns of the transmitted beam hold similar contours to the incident beam when the incident angle is small. Such contours would be ruined gradually with the increase of the incident angle.

Tables 1 and 2 show the values of Pol of the reflected and transmitted beams with different incident angles for three kinds of polarization modes. Cases 1, 2, and 3 stand for the x, circular, and radial polarizations, respectively.

Table 1. Pol of the reflected beam with different incident angles.

Reflected beam	Incident angle		
Three cases	$\beta = 10°$	$\beta = 20°$	$\beta = 30°$
Pol (case 1)	16.44	11.52	8.75
Pol (case 2)	–0.87	–0.83	–5.24
Pol (case 3)	–0.42	0.27	–3.80

Table 2. Pol of the transmitted beam with different incident angles.

Transmitted beam	Incident angle		
Three cases	$\beta = 10°$	$\beta = 20°$	$\beta = 30°$
Pol (case 1)	19.33	14.00	12.10
Pol (case 2)	–0.20	–0.67	–0.68
Pol (case 3)	0.50	1.45	2.26

It reveals in Tables 1 and 2 that the values of Pol for the x polarization incidence decrease as the incident angle increases, which means that there is more energy transmitting into the electric field component $E_{y\xi}$ from $E_{x\xi}$, reaching an agreement with the change trend as shown in Figs. 3 and 6. As for the circular polarization incidence, the polarization mode of the transmitted beam has a similar behavior to that of x polarization incidence, but the negative value of Pol indicates that the energy of electric field component E_{yt} is always higher than E_{xt}. In addition, the reflected beam whose value of Pol first rises to -0.83 from -0.87 and then drops to -5.24, goes through a non-monotonic transformation of polarization modes. Compared to the circular polarization incidence, the transformation trend of polarization modes of the reflected beam for the radial polarization incidence is similar, but the variation of the transmitted beam is just opposite.

3.3. Comparison of OAM states of the reflected and transmitted beams

The transformation of polarization modes finely reflects the energy transfer along the polarization directions. However, for practical applications of vortex beams, the investigation into the energy of each helical harmonic is important as well, especially in an OAM multiplexing system. To analyze the effects of polarization modes and incident angles on the deformation of OAM states, figures 12 and 13 plot the distributions of OAM states of the reflected and transmitted beams, respectively.

Figures 12 and 13 illustrate that as the incident angle increases, there are more adjacent OAM states derived in the reflected and transmitted beams, and the distributions of OAM states of the reflected beam are more complicated than those of the transmitted beam. The reflected beams for the x and circular polarization incidences have only single predominant OAM state $-l$ whose value is opposite to that of the transmitted beams l. However, the reflected beam for the radial polarization incidence has double predominant OAM states $(-l\ -1)$ and $(-l\ +1)$, and the corresponding predominant OAM states of the transmitted beam are $(l\ +1)$ and $(l\ -1)$, which brings into the correspondence with the analytic expression of the radially polarized Bessel vortex beam.[50] The negative predominant OAM states of the reflected beam can be interpreted by the reflection effect of vortex beams, which can be applied to the data swapping.[51] For the reflected beam, the energy of predominant OAM states firstly decreases and then increases as the incident angle gets bigger, and the energy of derived OAM states is gradually away from the predominant OAM state, which will cause fewer crosstalk problems. Instead, in the transmitted beam, the energy of predominant OAM states keeps a continuous consumption as the incident angle increases. Furthermore, the polarization modes of the incident beam have significant influences on the distributions of OAM states of the reflected and transmitted beams. The most obvious difference is the number of the predominant OAM state. At the same incident angle, the OAM state distribution of the reflected beam presents symmetric bar graphs centered on the OAM state $-l$, with two predominant states for radial polarization incidence and similar structures between x and circular polarization incidences. However, such symmetric structures are ruined in the transmitted beam for the case of circular polarization incidence. The most mentionable point is that the energy of the derived OAM states in transmitted beam for the radial polarization incidence focuses on the OAM state l, which is beyond our expectation.

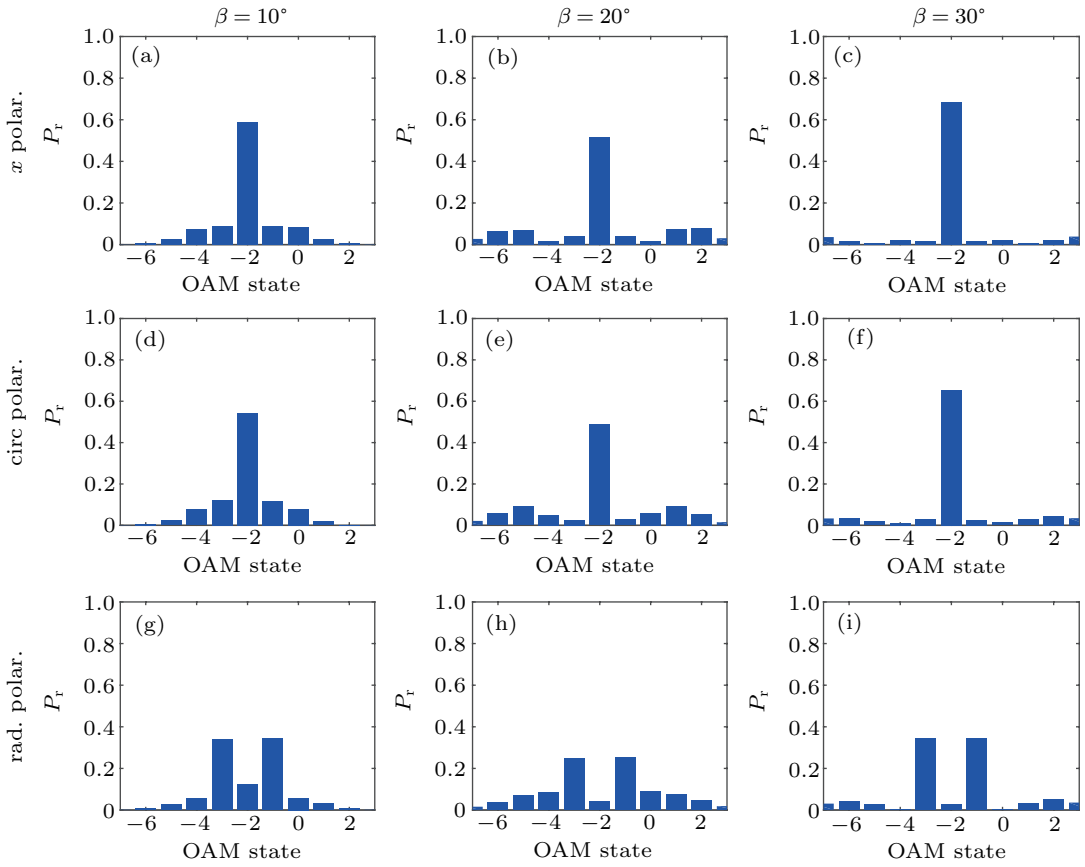


Fig. 12. OAM states of the reflected beam with different incident angles and polarization modes.

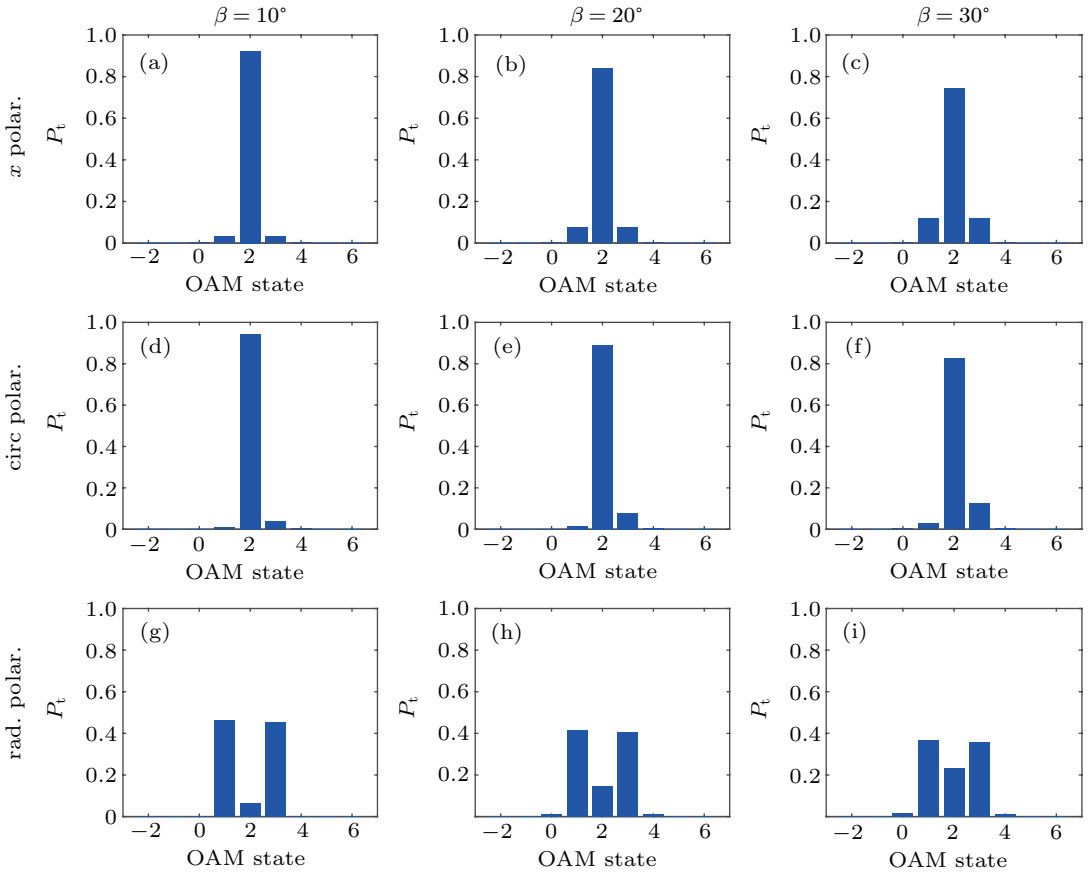


Fig. 13. OAM states of the transmitted beam with different incident angles and polarization modes.

4. Conclusions

The reflection and transmission of a PBVB by a uniaxial anisotropic slab had been investigated by use of the cylindrical vector wave function expansions. The electromagnetic fields of the incident, reflected, and transmitted beams, as well as their corresponding expansion coefficients, were obtained utilizing the CVWFs. The magnitude profiles of the field components, the transformation of polarization modes, and the distributions of OAM states of the reflected and transmitted beams were analyzed in detail. The results indicated that the magnitude profiles of the reflected field components were more obviously complicated than those of the transmitted field components, and their contours are seriously distorted as the incident angle increases. Compared to x and radial polarization incidences, the reflected beam for the circular polarization incidence had the minimum transformation of polarization modes between the transverse electric field components. Although the magnitude profiles of the reflected field components for three kinds of polarization modes were in wild disorder with a bigger incident angle, the energy of the reflected beam seemed to go back to the predominant OAM states. Different from the cases of x and circular polarization incidences, the derived OAM states in the transmitted beam for the radial polarization incidence located at the OAM state between its two predominant OAM states, leading to the focused effect of OAM state. The results in this paper may provide some supports in the design of optical devices and the OAM multiplexing communication combining with a polarization–division multiplexing segment.

References

[1] Allen L, Beijersbergen M W, Spreeuw R J and Woerdman J P 1992 *Phys. Rev. A* **45** 8185

[2] Wang C, Shao Q, Liu T, Ren Y 2018 *Optical Precision Manufacturing, Testing and Applications* **10847** 1084703

[3] Ruffato G, Massari M and Romanato F 2014 *Opt. Lett.* **39** 5094

[4] Novitsky A V and Barkovsky L M 2008 *J. Opt. A-Pure. Appl. Opt.* **10** 075006

[5] Zhou Z, Guo Y and Zhu L 2014 *Chin. Phys. B* **23** 044201

[6] Belyi V N, Khilo N A, Kazak N S, Ryzhevich A A and Forbes A 2011 *Opt. Eng.* **50** 059001

[7] Bozinovic N, Yue Y, Ren Y, Tur M, Kristensen P, Huang H, Willner A E and Ramachandran S 2013 *Science* **340** 1545

[8] Yan L, Gregg P, Karimi E, Rubano A, Marrucci L, Boyd R and Ramachandran S 2015 *Optica* **2** 900

[9] Rui G, Gu B, Zhan Q and Cui Y 2016 *Prog. Electromagn. Res. Symp. (PIERS)* pp. 738–739

[10] Gibson G, Courtial J, Padgett M J, Vasnetsov M, Pas'ko V, Barnett S M and Franke-Arnold S 2004 *Opt. Express* **12** 5448

[11] Wang J, Li S, Luo M, Liu J, Zhu L, Li C, Xie D, Yang Q, Yu S and Sun J 2014 *Eur. Conf. Opt. Commun. (ECOC)* pp. 1–3

[12] Wang J, Liu J, Lv X, Zhu L, Wang D, Li S, Wang A, Zhao Y, Long Y and Du J 2015 *Eur. Conf. Opt. Commun. (ECOC)* p. 1

[13] Chaudhary S and Amphawan A 2018 *Photon. Netw. Commun.* **35** 374

[14] Huang H, Xie G, Yan Y, Ahmed N, Ren Y, Yue Y, Rogawski D, Willner M J, Erkmen B I, Birnbaum K M, Dolinar S J, Lavery M P, Padgett M J, Tur M and Willner A E 2014 *Opt. Lett.* **39** 197

[15] Zhu L, Zhu G, Wang A, Wang L, Ai J, Chen S, Du C, Liu J, Yu S and Wang J 2018 *Opt. Lett.* **43** 1890

[16] Djordjevic I B, Zhang S L and Wang T 2017 *13th International Conference on Advanced Technologies, Systems and Services in Telecommunications (Telsiks)* p. 317

[17] Sun T F, Liu M W, Li Z X, Li Y C, Zhang Q W and Wang M 2017 *Opto-Electron. Commun. Conf. (Oecc) Photon. Global Conf. (Pgc)* p. 1

[18] Ndagano B, Nape I, Cox M A, Rosales-Guzman C and Forbes A 2018 *J. Lightwave Technol.* **36** 292

[19] Zhao M, Gao X, Xie M, Qian J, Song C and Huang S 2018 *Opt. Commun.* **426** 126

[20] Stoian R, Bhuyan M K, Zhang G, Cheng G, Meyer R and Courvoisier F 2018 *Adv. Opt. Technol.* **7** 165

[21] Djordjevic I B 2011 *Opt. Express* **19** 14277

[22] Yu W H, Zhao R H, Deng F, Huang J Y, Chen C D, Yang X B, Zhao Y P and Deng D M 2016 *Chin. Phys. B* **25** 044201

[23] Wang L Y, Zhang J B, Feng L Y, Pang Z H, Zhong T F and Deng D M 2018 *Chin. Phys. B* **27** 054103

[24] Lo Y L and Yu T C 2006 *Opt. Commun.* **259** 40

[25] Lu K and Saleh B E 1990 *Opt. Eng.* **29** 240

[26] Chugunov Y V, Shirokov E A and Fomina I A 2015 *Radiophys. Quant. EL +* **58** 318

[27] Li H Y, Liu J W, Bai L and Wu Z S 2018 *Appl. Opt.* **57** 7353

[28] Durnin J, Miceli J Jr and Eberly J H 1987 *Phys. Rev. Lett.* **58** 1499

[29] Zhang Y L, Ma D L, Yuan X H and Zhou Z Y 2016 *Appl. Opt.* **55** 9211

[30] Chen B Y, Huang X S, Gou D Z, Zeng J Z, Chen G Q, Pang M J, Hu Y H, Zhao Z, Zhang Y F, Zhou Z, Wu H T, Cheng H P, Zhang Z G, Xu C, Li Y L, Chen L Y and Wang A M 2018 *Biomed. Opt. Express* **9** 1992

[31] McGloin D, Garces-Chavez V and Dholakia K 2003 *Opt. Lett.* **28** 657

[32] Volke-Sepulveda K, Garces-Chavez V, Chavez-Cerda S, Arlt J and Dholakia K 2002 *J. Opt. B-Quantum S. O.* **4** S82

[33] Birch P, Ituen I, Young R and Chatwin C 2015 *J. Opt. Soc. Am. A* **32** 2066

[34] Collett E 1971 *Am. J. Phys.* **39** 1483

[35] Wang J, Yang J Y, Fazal I M, Ahmed N, Yan Y, Huang H, Ren Y X, Yue Y, Dolinar S, Tur M and Willner A E 2012 *Nat. Photon.* **6** 488

[36] Yasa U G, Turduev M, Giden I H and Kurt H 2017 *J. Lightwave Technol.* **35** 1677

[37] Quabis S, Dorn R, Eberler M, Glockl O and Leuchs G 2000 *Opt. Commun.* **179** 1

[38] Nesterov A V and Niziev V G 2001 *J. Opt. B-Quantum S. O.* **3** S215

[39] King T A, Hogervorst W, Kazak N S, Khilo N A and Ryzhevich A A 2001 *Opt. Commun.* **187** 407

[40] Fu S, Zhang S and Gao C 2016 *Sci. Rep-Uk* **6** 30765

[41] Mitri F G, Li R X, Guo L X and Ding C Y 2017 *J. Quantum Spectrosc. Radiat. Transfer* **187** 97

[42] Chen J, Ng J, Wang P and Lin Z F 2010 *Opt. Lett.* **35** 1674

[43] Ma X B and Li E B 2010 *Chin. Opt. Lett.* **8** 1195

[44] Gouesbet G, Wang J J and Han Y P 2010 *Opt. Commun.* **283** 3235

[45] Zhang H Y and Han Y P 2008 *J. Opt. Soc. Am. B* **25** 255

[46] Wang M J, Zhang H Y, Liu G S, Li Y L and Dong Q F 2014 *Opt. Express* **22** 3705

[47] Li H Y, Honary F, Wang J J, Liu J W, Wu Z S and Bai L 2018 *Appl. Opt.* **57** 1967

[48] Jiang Y S, Wang S H, Zhang J H, Ou J and Tang H 2013 *Opt. Commun.* **303** 38

[49] Wang J J, Wriedt T, Lock J A and Madler L 2016 *J. Quantum Spectrosc. Radiat. Transfer* **184** 218

[50] Wang J J, Wriedt T, Lock J A and Jiao Y C 2017 *J. Quantum Spectrosc. Radiat. Transfer* **195** 8

[51] Yue Y, Huang H, Ahmed N, Yan Y, Ren Y X, Xie G D, Rogawski D, Tur M and Willner A E 2013 *Opt. Lett.* **38** 5118